JOC The Journal of Organic Chemistry

Featured Article

pubs.acs.org/joc

Elucidation of the Mechanism of the Reaction between Phenylboronic Acid and a Model Diol, Alizarin Red S

John W. Tomsho and Stephen J. Benkovic*

Department of Chemistry, The Pennsylvania State University, 414 Wartik Laboratory, University Park, Pennsylvania 16802, United States

Supporting Information

ABSTRACT: In this work, the reaction between phenylboronic acid and the diol-containing, fluorescent dye Alizarin Red S (**ARS**) was probed. Fluorescence titrations, ^{11}B NMR measurements, and both pre- and steady-state kinetic experiments were used for the characterization of this reaction over a large pH range (4−10.5). It was shown that **ARS** preferentially reacted with the boronic (neutral, trigonal) form of phenylboronic acid; however, the boronate (anionic, tetrahedral) form was also reactive. All in all, four reactant species were implicated in the formation of four different adduct species. The rate of a given adduct formation depended on the combination of the solution pH and the pK_a's of both **ARS** and the arylboronic acid. The reaction was found to proceed in two distinct kinetic steps with the products and starting materials in facile exchange. In addition, the elucidation of the mechanism indicated the presence of two fluorescent products with the structure of the major contributor differing from what had been cited in the literature.

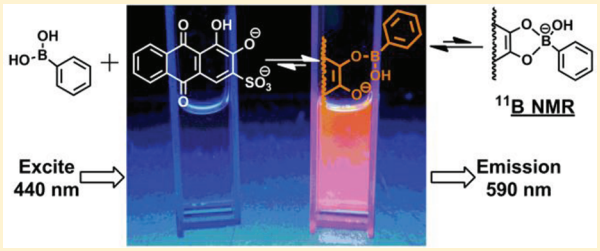

INTRODUCTION

The reversible binding of diol-containing compounds to arylboronic acids, such as phenylboronic acid (**1**), has been studied for over 50 years. Since the first report by Lorand and Edwards,[1] boronic acids have been exploited extensively for sensing applications, including carbohydrates, metals, and anions.[2−6] Boronic acids are Lewis acids that exist as either a neutral, trigonal-planar species at low pH or a negatively charged, tetrahedral boronate species at high pH (Figure 1). The early consensus in the field indicated

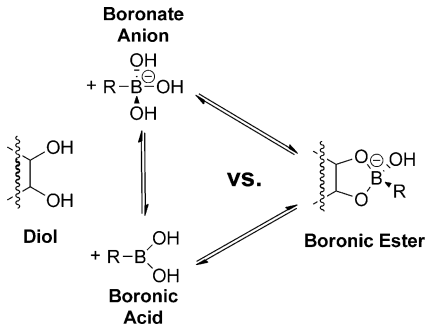

Figure 1. Boronic acid reactivity question: Which is the reactive species, the acid, the boronate anion, or both?

that bidentate ester formation between boronic acids and diols proceeded with the boronate anion as the reactive species.[2] This conclusion was based on findings that boronic ester formation was favored at high pH[1,7−10] and by kinetic studies that indicated the boronate ion was the kinetically favored reactive species by a factor of at least 10^3−10^4.[11−13] However, recent work drew this hypothesis into question by demonstrating that the neutral boronic acid is the predominantly reactive species in solution.[14−17]

In addition to their uses as molecular sensors, boronic acids have many pharmaceutically useful properties.[2,18−22] Besides acting as inhibitors of the proteasome (Velcade),[23] boronic acids also inhibited serine proteases (including β-lactamases,[24] hepatitis C virus protease,[25] and thrombin[26]), autotaxin,[27] and arginase,[28] among others.[29−31] In contrast to the ester formation with diols, reactions between boronic acids and active site nucleophiles usually yield monodentate enzyme complexes.[2] However, there have been reports of bi- and tridentate active site complexes as well. In one case, a substituted benzoxaborole formed a tight-binding complex with the terminal ribosyl diol of tRNA on a fungal leucyl tRNA synthetase.[32] A tridentate complex was observed between a substituted methylboronic acid, two serine Oγ's, and a terminal N of a lysine residue.[33] In both of these cases, time-dependent enzyme inhibition kinetics were noted. We conjectured that detailed research into the reactivity of boronic acids with nucleophiles under physiologically relevant conditions could yield insights to further the development of these compounds as pharmaceutical agents.

In this work, the reaction between phenylboronic acid (**1**) and the diol-containing, fluorescent dye Alizarin Red S (**ARS**) was probed (Figure 2). **ARS** is a readily available dye that showed a dramatic increase in fluorescence when complexed with boron in aqueous solutions at near physiological pH.[34−36] Its use has since been expanded to many sensing applications in near-neutral, aqueous media via fluorescence.[9,37−39] Fluorescence

Received: November 1, 2011
Published: January 3, 2012

   dx.doi.org/10.1021/jo202250d | J. Org. Chem. 2012, 77, 2098−2106

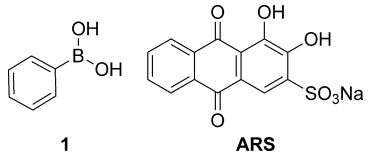

Figure 2. Structures of phenylboronic acid (**1**) and Alizarin Red S (**ARS**).

titrations, ^{11}B-NMR measurements, and both pre- and steady-state kinetic experiments were used for the characterization of this reaction over a large pH range (4−10.5). It was shown that although **ARS** reacted with both the boronic (neutral, trigonal) form as well as the boronate (anionic, tetrahedral) form of **1** the boronic pathway is preferred. All in all, four reactant species were implicated in the formation of four different adduct species. The rate of adduct formation depended on the combination of the solution pH and the pK_a's of both **ARS** and the arylboronic acid. The reaction was found to proceed in two distinct kinetic steps with the products and starting materials in facile exchange. In addition, the elucidation of the mechanism indicated the presence of two fluorescent products with the structure of the major contributor differing from what had been cited in the literature.

RESULTS AND DISCUSSION

In all of these experiments, buffer selection was an important consideration. The first criterion was to avoid potential interference by boronic acid interactions with common, diol-containing buffers such as Tris and Bis-tris propane (adduct formation confirmed by ^{11}B NMR, data not shown). Other, less obvious interactions have been shown between boronic acids and phosphate, citrate, and imidazole buffer systems;[9,40] therefore, these systems were also removed from consideration. It was reported that HEPES buffer did not affect the **1**:**ARS** interaction so it and other members of the Good family of buffers[41] were chosen for use in these studies. Adduct formation was not detected at any pH with any of the Good buffers during ^{11}B NMR experiments. Control experiments in which the buffer concentration (MES, pH = 5.5) was varied from 25 to 100 mM showed no significant change in apparent rate (data not shown). It is important to note that because of the difference in choice of buffer system composition, the results obtained in this work may, in some cases, vary significantly from those previously reported in literature which utilized many of the boron-interacting buffers.

Steady-State Analysis. Exploration of the reaction between **1** toward the **ARS** diol began with the determination of the fluorescence spectra of **ARS** and the adduct, **1**:**ARS**, with solution pH ranging from 1 to 13. **ARS** itself has little fluorescence regardless of pH as can be seen in Figure 3. The adduct, however, yielded a large increase in fluorescence with an excitation maxima at 464 ± 5 nm and an emission maxima at 590 ± 5 nm. The fluorescence was found to be heavily dependent on solution pH with a broad pH range of near maximum, from 6.5 to 8.5. It was observed that both the emission and excitation spectra of the adduct did not significantly change in shape from pH 4−10 indicative of a single, major fluorescent species being formed across this wide range of pH (data not shown).

Equation 1 is a two pK_a equation for the fitting of fluorescence data in Figure 3. The equation is derived from a model where three species are in an equilibrium connected by two ionizations with only the middle species contributing to the

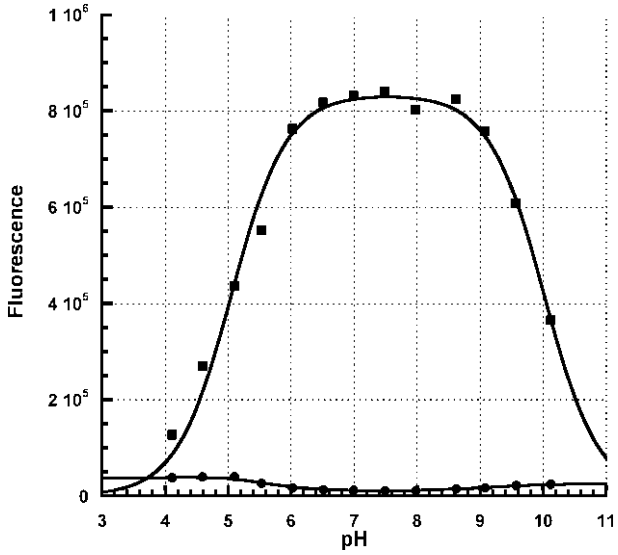

Figure 3. Fluorescence vs pH for **ARS** (●) and **1**:**ARS** (■). Excitation was at 440 nm, while emission was monitored at 565 and 590 nm, respectively. The fluorescence at pH = 1 and 13 was similar and small for both solution sets and is not shown for clarity. Data for **1**:**ARS** were fit to a two-pK_a equation, eq 1, and resulted in pK_a's of 5.0 and 10.0.

fluorescent signal (see Figure 8). It is assumed that the fluorescence signal is directly proportional to the concentration of the fluorescent species, [fluorescent species]. The equation is placed in terms of the total concentration of ARS, $[ARS]_T$, observed ionization constants (pK_{a1} and pK_{a2}), and solution pH.

$$[\text{fluorescent species}] = \frac{[ARS]_T \cdot 10^{(pK_{a2}-pH)}}{1 + 10^{(pK_{a2}-pH)} + (10^{(pK_{a1}-pH)} \cdot 10^{(pK_{a2}-pH)})} \quad (1)$$

The fluorescence vs pH data for **1**:**ARS** in Figure 3 were fit to a two-pK_a equation, eq 1, which describes a fluorescence increase followed by a decrease as a function of increasing solution pH. The apparent pK_a's for the **1**:**ARS** adduct via fluorescence were found to be 5.0 ± 0.2 and 10.0 ± 0.2. For comparison, the pK_a's of **1**:**ARS**, **1**, and **ARS** were determined utilizing UV/vis spectrophotometry; see the Supporting Information for data. With this method, the adduct pK_a's were found to be similar with values of 4.7 ± 0.1 and 11.0 ± 0.1. The pK_a of **1** was determined to be 9.2 ± 0.1 under these conditions, while **ARS** ionizations were found to occur at 6.0 ± 0.1 and 11.0 ± 0.1. These data compare well with those previously reported in the literature as 8.8, for **1** in phosphate buffer,[10] and 4.5−5.3 and ∼11 for **ARS**.[37,42] Comparison of the individual component pK_a's versus those of the adduct is informative. The pK_{a1} ∼ 5 indicates that the fluorescent adduct has a pK_a lower than that of the free **ARS**. In addition, these data are consistent with the major reactive species being the neutral, trigonal form of **1** and the monoanionic **ARS**. The loss of fluorescence at high pH, as reflected in the pK_{a2}, may be due to adduct instability as has been proposed previously.[9]

To further characterize the nature of the fluorescent species, fluorescence lifetime measurements were taken across a pH range of 4−10. Consistent with the above results, the lifetime measurements revealed a major fluorescent species (82−92%, τ1 = 0.55 ns) as well as another, minor, contributor (8−18%,

dx.doi.org/10.1021/jo202250d | J. Org. Chem. 2012, 77, 2098−2106

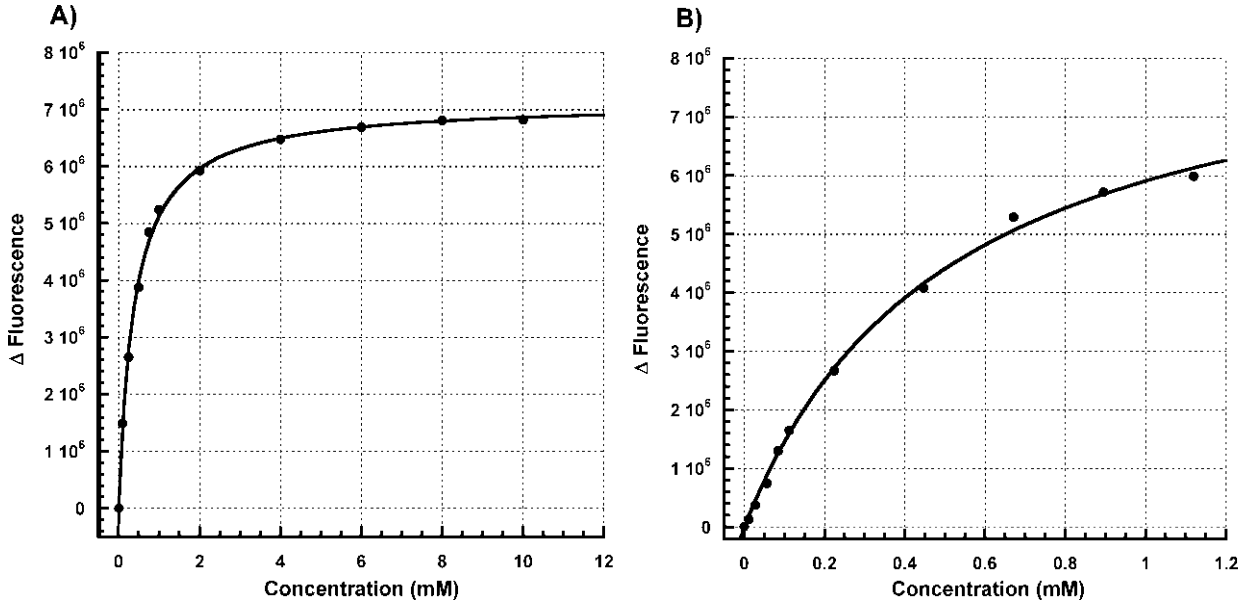

Figure 4. Steady-state fluorescence titration of **ARS** with **1** for the determination of the association constant via fitting to eq 2 (solid lines) at (A) pH 7.0, K_a = 2550 ± 95 M^{-1} and (B) pH 10.1, K_a = 1940 ± 160 M^{-1}, after adjustment for concentration of neutral, trigonal **1** in solution.

$\tau 2$ = 1.9 − 2.6 ns). Though the relative ratios of the two species changed somewhat with pH, the lifetime of the major contributor remained constant across the examined range. In contrast, the lifetime of the minor contributor shifted from 2.6 ns (pH = 4) to 1.9 ns (pH = 9) as the pH was increased, suggesting the presence of two different species connected by an ionization.

The next consideration was the determination of the binding affinity of **1** for **ARS** in solutions of varying pH. Solution pH values of 7 and 10 were initially chosen to probe the association of **1** with the monoanionic form of **ARS**. The change in fluorescence was plotted against neutral, trigonal boron compound concentration, and the resulting data were fit with nonlinear least-squares analysis to obtain the K_a's, Figure 4. Comparison of the binding affinities (Table 1) at low and high pH reveals a nearly identical affinity, 2550 and 1940 M^{-1} at pH = 7 and 10, respectively, toward **ARS** if only the boronic acid form is considered reactive in solution. These results run counter to the prevailing notion that boronic ester formation is favored at high pH.[1,7−10] This, however, may be attributed to charge−charge repulsion between the anionic **ARS** diol with the tetrahedral boronate. These results would be consistent with the findings of van Duin, et al. that found that the optimum pH for ester formation between boric acid (pK_a = 9.1) and glycolic acid (pK_a = 3.8) was ∼7, between the ligand's and boron's pK_a values.[7] It is noted, however, that the glycolic acid offers a deprotonated carboxylic acid rather than the deprotonated alcohol of **ARS** as the anionic functionality. Equation 2 shows K_a determination by two-component fluorescent titrations, following the method of Springsteen and Wang[9] where Δfluorescence is the observed change in fluorescence, $[B]_T$ is the total concentration of boron species, and $Fluor_{max}$ is the maximum change in fluorescence.

$$\Delta\text{fluorescence} = \frac{[B]_T \cdot \text{Fluor}_{max}}{(1/K_a) + [B]_T} \quad (2)$$

Table 1. Comparison of Adduct Formation of 1 with ARS in Aqueous Solution, pH 5−10, via Fluorescence and ^{11}B NMR Methods[b]

	fluorescence	^{11}B NMR
pH	K_{a1} (M^{-1})	K_2
5.0	ND	0.24 ± 0.04
6.0	ND	0.43 ± 0.03
7.0	2550 ± 95	0.46 ± 0.05
8.0	ND	0.50 ± 0.01
9.0	ND	0.57 ± 0.13
10.0	1940 ± 160	ND[a]

[a]Under these particular conditions, two peaks are evident, but significant peak overlap precludes accurate integration. [b]ND = not determined.

^{11}B NMR has been used in a number of studies to elucidate the configuration about the boron atom in solution.[7,12,14,43−45] In these experiments, boronic acids with differing geometries about the boron atom (i.e., trigonal, tetrahedral, and diol adducts) have unique chemical shifts. In cases in which two species interchange faster than the NMR time scale, a single peak that represents the weighted average of the two species is observed. This was the case for the simple acid−base equilibria of the boronic acids in which the trigonal and tetrahedral forms are in rapid exchange, so that experiments in which the chemical shift is measured at different solution pH's may be used to obtain the pK_a of boronic acids.[46] However, if the exchange is slow compared with the NMR time scale (slower than ∼0.1 s^{-1}), multiple peaks are observed, Figure 5. This is generally the case with boronic acid:diol adducts and has allowed the measurements of the binding of **ARS** to **1** at solution pH ranging from 5 to 9.

The most interesting observation comes upon inspection of the NMR results at pH = 7. It was immediately evident that there was insufficient product formation detected given the initial compound concentrations and the K_a from the fluorescent titrations. If the binding constant was calculated based

dx.doi.org/10.1021/jo202250d | J. Org. Chem. 2012, 77, 2098−2106

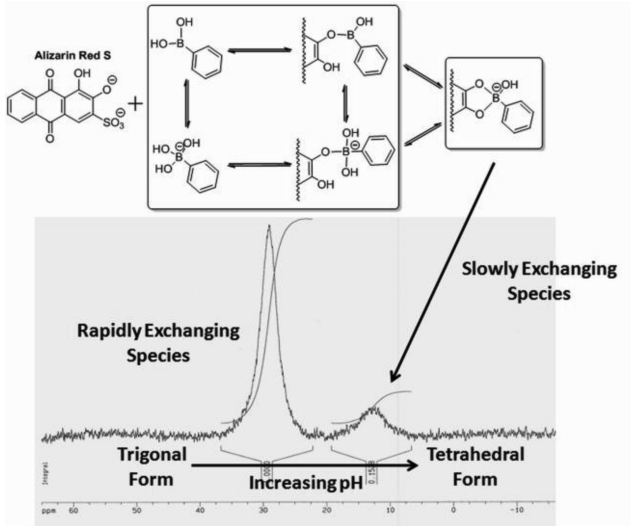

Figure 5. Example of ^{11}B NMR results in which two peaks are observed. One peak results from the rapid interconversion between the trigonal and tetrahedral geometries about boron, while the other peak is attributed to the slowly exchanging, cyclic tetrahedral adduct.

solely on the NMR data, a 50-fold difference in K_a between this and the fluorescence titration methods was noted. The simplest explanation for this inconsistency is that the two methods are measuring two different species, with the NMR method capturing an anionic, tetrahedral, bidentate adduct between **1** and **ARS** (based upon the ^{11}B chemical shift) as illustrated in Figure 6. With this being the case, it is still possible to calculate K_2, relating the intermediate adduct (fluorescent adduct, Figure 6) and the final, cyclic adduct (^{11}B NMR adduct, Figure 6). It is assumed that the reaction has proceeded to the extent that intermediate adduct is completely formed and that the NMR integration results are reporting only on the excess free **1**, intermediate adduct, and final cyclic adduct. Thus, K_2 may be calculated by dividing the concentration of the final cyclic adduct by the difference between the limiting reagent and final cyclic adduct concentrations. The results are summarized and compared with the data obtained from the fluorescence method in Table 1. The complete data and further discussion on this calculation has been included in the Supporting Information. Examination of these results reveals that the binding is nearly constant across pH (less than a 3-fold difference in binding over a 4 orders of magnitude change in $[H^+]$) and indicates that, at equilibrium, the final, cyclic adduct concentration is approximately 50% of the intermediate adduct.

The structures proposed in Figure 6 and subsequently in this work have taken in to account much of the existing literature. Initially, there was concern that an oxygen of the sulfonic acid on ARS might play a role in the interaction with the boronic acid. This idea was discarded after comparison of alizarin–phenylboronic acid fluorescence in methanol and ARS–phenylboronic acid in neutral, aqueous solution.[38,47] In both cases, nearly identical changes in fluorescence emission and UV/vis absorption were found. Additionally, the experiments reported herein utilized Good buffers, which all contain a sulfonic acid moiety, and no buffer concentration effect on reaction rate was found. Next, it was determined that the hydroxyl group proximal to the sulfonic acid group will be deprotonated first due to its lower pK_a. The distal hydroxyl group is involved in an intramolecular hydrogen bond with the keto oxygen resulting in the more ready elimination of the proton from the proximal hydroxyl.[48,49] Once deprotonated, this species will be responsible for the attack on boron thereby yielding the major fluorescent adduct illustrated Figure 6.

The cumulative results of these experiments implicate the neutral, trigonal boronic acid as the reactive species in ester formation with a monoanionic diol at near-neutral pH. However, the collective results from the fluorescent lifetime, fluorescent titrations, and ^{11}B NMR experiments support the conclusion that two products exist in equilibrium, related by K_{a1} and K_2, as shown in Figure 6. The end product has been assigned as the diester, spiro about boron, based upon the NMR shift. Since the NMR experiments indicate a much lower overall K_a (from **1** and **ARS**), this product is the minor contributor to fluorescence observed in the fluorescence lifetime experiments. With the final product resulting from the loss of two water molecules, the intermediate product is derived from a single dehydration step. This intermediate adduct is then assigned as the major fluorescent product. These assignments are consistent with the proposed molecular structures since the major fluorescent contributor will be largely planar and containing a trigonal boron whose empty p-orbital has been known to extend conjugation.[50−52] Meanwhile, the minor contributor will have a nonplanar structure and a boron atom with a filled p-orbital, both contributing to the lesser observed fluorescence signal for this molecule. Indeed, the latter structure has previously been assumed to be the sole product giving rise to the observed fluorescence.

Presteady-State. The recent analysis of the equations which would describe whether the neutral boronic acid or the anionic tetrahedral boronate is the predominantly reactive species in solution by Rietjens and Steenbergen[15] illuminate two major considerations about the determination of the reactive species. First, the thermodynamic equations which describe the two cases are equivalent and therefore thermodynamic analyses cannot distinguish between them. Kinetic equations describing the two cases, however, are not equivalent and the equations describing the boronic acid as the reactive species should be dependent on pH. Therefore, we undertook presteady state kinetic experiments with fluorescence detection to monitor the reaction between **1** and **ARS**

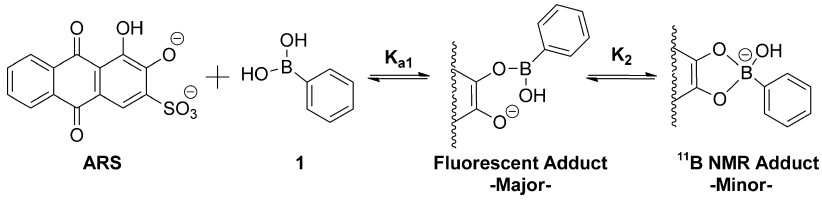

Figure 6. Minimal mechanistic proposal for near-neutral solution pH, based upon the combination of all steady-state data.

dx.doi.org/10.1021/jo202250d | J. Org. Chem. 2012, 77, 2098–2106

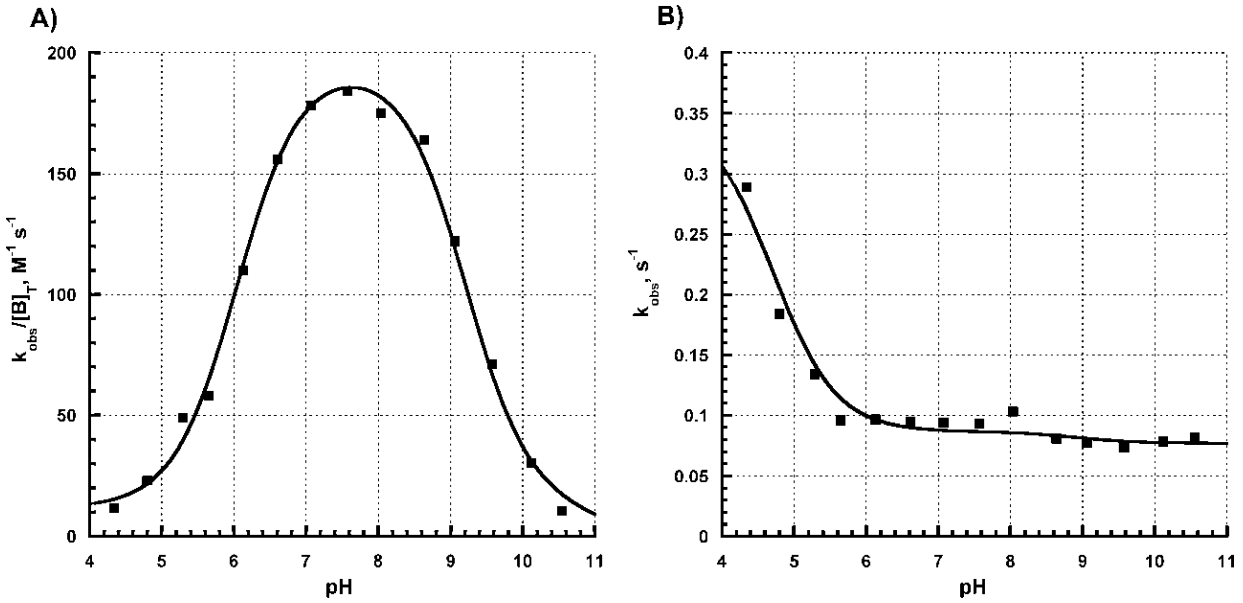

Figure 7. Analysis of stopped-flow pH profiles of k_{on} and k_{off} enable partial mechanism elucidation: (A) forward rate data are fit to eq 4; (B) reverse rate data are fit to eq 6.

over a wide range of pH (4−10.5) to elucidate the kinetic mechanism of the reaction.

Solutions of **1** and **ARS** were prepared in otherwise identical solutions containing buffers at various, matched pH's. Pseudofirst-order conditions were utilized with [**ARS**] being fixed and limiting while [**1**] was in excess and varied. The reaction was initiated by rapid mixing of the reagents and reaction progress was monitored by fluorescence detection. The resultant progress curves were adequately fit by a single exponential to obtain an apparent rate. These data, for each pH, were then replotted vs [**1**] and subjected to linear fitting to obtain the on (formation) and off (dissociation) rates (slope, k_{+1} and y-intercept, k_{-1}, respectively) of the reaction.

The forward and reverse rate data thus obtained were plotted vs pH and fit to equations describing the reaction paths with changing pH, Figure 7. The equations were developed by inspection of the data and the generation of models of increasing complexity. The simplest model that adequately described the data required three single-step, parallel reactions yielding three distinct adduct products as shown in Figure 8. In the forward direction, the observed rate was explained by the following equation:

$$v = (k_1[B_1] + k_2[B_2])[A_1] + k_3[B_1][A_0] \quad (3)$$

where B_1 = neutral, trigonal **1**; B_2 = anionic, tetrahedral **1**; A_0 = **ARS** with alcohols protonated; A_1 = **ARS** with a single deprotonated alcohol; A_2 = **ARS** with both alcohols of the diol deprotonated; and k_1−k_3 representing the forward rates of the respective reactions. The reactivity of A_2 did not need to be considered. Equation 3 was then recast in terms of the total concentrations of **1** and **ARS** ($[B]_T$ and $[A]_T$, respectively) and introduction of the pK_a's for the acid/base behavior of the species B_1 and B_2 (K_1^B) and A_0, A_1, and A_2 (K_1^A and K_2^A, respectively). The resulting equation follows:

$$\frac{k_{obs}}{[B]_T} = \frac{v}{[A]_T[B]_T} = \left(\frac{(k_1[H^+]) + (k_2K_1^B)}{K_1^B + [H^+]}\right)\left(\frac{K_1^A[H^+]}{[H^+]^2 + ([H^+]K_1^A) + (K_1^AK_2^A)}\right) + k_3\left(\frac{[H^+]}{K_1^B + [H^+]}\right)\left(\frac{[H^+]^2}{[H^+]^2 + ([H^+]K_1^A) + (K_1^AK_2^A)}\right) \quad (4)$$

In the reverse reaction, the rate depends on the dissociation of the three adduct species, P_1, P_2, and P_3, that are connected by two ionization steps, K_1^P and K_2^P respectively.

$$v = k_{-1}[P_2] + k_{-2}[P_3] + k_{-3}[P_1] \quad (5)$$

Equation 5 was then recast in terms of the total concentrations of adducts ($[P]_T$) and solution pH with the dissociation constant for P_2 to P_1 (K_1^P) being determined from the steady-state UV analysis of the adduct ionization and K_2^P being determined during fitting of the rate data. Thus, the resulting eq 6 follows:

$$k_{obs} = \frac{v}{[P]_T} = \frac{(k_{-1}[H^+]K_1^P) + (k_{-2}K_1^PK_2^P) + (k_{-3}[H^+]^2)}{[H^+]^2 + ([H^+]K_1^P) + (K_1^PK_2^P)} \quad (6)$$

The calculated rate constants for the various steps are shown in Figure 8. Support for the validity of this model comes from several considerations. First the affinity constant K_{a1} calculated from the rates agree well with those obtained in the steady state fluorescent titrations at pH = 7. Second, in order to assign

dx.doi.org/10.1021/jo202250d | J. Org. Chem. 2012, 77, 2098−2106

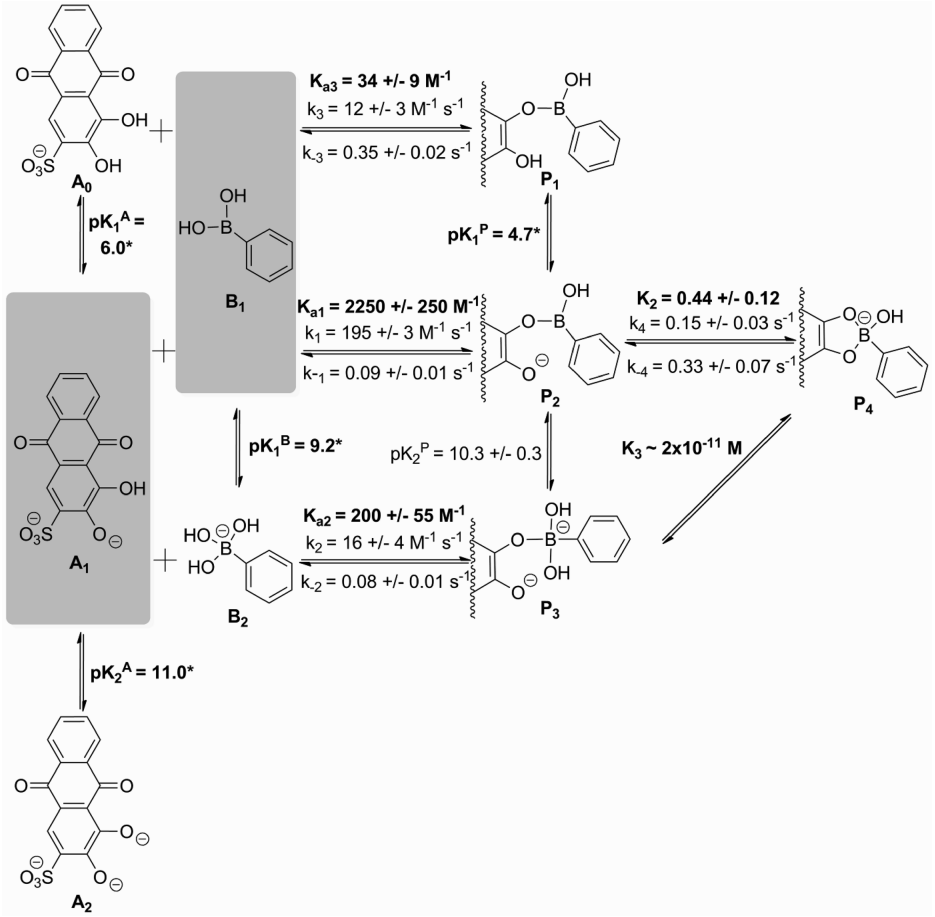

Figure 8. Elucidated mechanism for the reaction between **1** and **ARS** in aqueous solution in pH ranging from 4 (top) to 10.5 (bottom). *Values were determined in an independent experiment(s).

probable structures to the three adduct species pH-jump experiments were completed. In these, the adduct was preformed in situ by premixing **1** and **ARS** at pH's between 6 and 9. A rapid pH change in the adduct solution was effected by rapidly mixing it with acid, base, or strongly buffered solutions. These experiments yielded two significant findings: (1) upon changing pH in either direction from near-neutral pH, there was an instantaneous (within instrument dead-time) UV/vis spectral shift noted (Supporting Information). These have been attributed to the ionization reactions depicted in Figure 8 with the first ionization being the deprotonation of the alcohol on the **1**:**ARS** monoester adduct, P_1 to P_2, and the second loss of water proton upon the hydroxylation of the boron, P_2 to P_3. (2) The rates obtained from the reaction progress as monitored by fluorescence are nearly identical to those obtained from the fitting of the data in Figure 7. In the pH-drop experiment where the pH was changed from 6 to 4, the observed rate was 0.39 s^{-1} neatly matching the fitting result of 0.35 s^{-1} for the back reaction of the protonated trigonal adduct, P_1. In a pH-jump experiment where the pH was changed from 7.5 to 13, the observed rate was 0.081 s^{-1} which is identical to the 0.08 s^{-1} obtained from fitting for the back reaction of the tetravalent boron species, P_3. Finally, support also comes from examination of the resulting thermodynamics. The top "thermodynamic box" (A_0 and B_1 to P_1 to P_2 to A_1 and B_1) reveals closure with the measurement errors taken into consideration. Also, the pK_2^P value is calculated by closure of the lower thermodynamic box. With the association constants of the other three arms (K_{a1}, K_{a2}, and pK_1^B) known, the pK_2^P value is calculated to be 10.3 ± 0.3. This value is reasonable since charge−charge repulsion would be expected to raise the pK_a significantly from the value of 9.2 measured for the equivalent ionization of free **1**. Experimentally this pK_a value is supported by the observation that the fluorescence plateau values of the titrations are nearly identical at pH = 7.0 and 10.1 (Figure 4).

Examination of the forward reaction rates elucidated by these kinetic data reveal an order of magnitude difference between the preferred reaction path, $A_1 + B_1 \rightarrow P_2$, versus the other two paths. This seems to indicate that the equilibrium formation of these products is predominately controlled by the initial association reaction. This preferred reaction occurs between the monodeprotonated **ARS** and the neutral, trigonal **1** species. This would be expected since, in this arrangement, the nucleophilic **ARS** oxyanion may freely attack the empty p-orbital of the neutral boronic acid. The other two paths are less favorable with reactions occurring between: the less nucleophilic ARS alcohol, A_0, and B_1 at low pH; and A_1 attacking the anionic, tetrahedral **1** species, B_2, having to overcome charge−charge repulsion at high pH.

The reverse reaction pH profile shows an increasing rate with decreasing pH indicative of the decomposition reaction through P_1 occurring at pH ≤ 5. Surprisingly, these kinetics studies also reveal that reverse reaction rates from species P_2 and P_3 are essentially unchanging from pH 6−10.5 while the pH-jump experiments extend this to pH 13. Given the proposed structure of the P_3 species, it was predicted that this species

dx.doi.org/10.1021/jo202250d | J. Org. Chem. 2012, 77, 2098−2106

would be less stable with a correspondingly higher k_{-2}. Since this was not observed, this may be indicative of internal stabilization of the product, P_3, via intramolecular hydrogen bonding. These observations also support the proposal that the formation of these adducts in aqueous solution is largely controlled by the initial association reaction.

The contributions of the full-ester, spiro adduct, P_4, seen in the ^{11}B NMR experiments were elusive owing to the lack of a definitive fluorescence or UV absorbance spectral assignment. To address this, the adduct was accessed synthetically in non-aqueous media and then introduced into aqueous solutions of various pH to monitor compound dissociation. The synthesis was achieved by reacting **1** and **ARS** in acetonitrile with anhydrous potassium carbonate serving as both a base and dehydrating agent. It was noted that this synthetic method yields a solution with about 180-fold excess free phenylboronic acid due to the poor solubility of **ARS**. Product synthesis was monitored by UV/vis and fluorescence spectral changes and confirmation obtained by NMR where ^{1}H NMR revealed the loss of both hydroxyl protons from ARS, and the ^{11}B NMR showed formation of a new peak with a shift consistent with a tetrahedral geometry about boron (Supporting Information).

Again, stopped-flow experiments were used to monitor the reverse reaction of the cyclization step. The prepared full-ester, spiro adduct in anhydrous acetonitrile was diluted 25-fold into aqueous buffer (pH 6−8) and the reaction progress followed by fluorescence. In all kinetic runs, a double exponential decay of fluorescence was noted. These data were fit to a double exponential with the second, slower rate constrained to the reverse reaction rate constant appropriate for that pH obtained from the above kinetics in order to determine the reverse rate constant for the second step (k_{-4}), Table 2. When these data

Table 2. Cyclization Step Reaction Rates

	rate (s^{-1})	
pH	k_4	k_{-4}
6.0	0.17 ± 0.02	0.39 ± 0.04
7.0	0.16 ± 0.02	0.35 ± 0.02
8.0	0.12 ± 0.01	0.25 ± 0.01

are combined with the previously determined binding constants from the ^{11}B NMR steady state experiments (Table 1, K_2) and the kinetics to the first adducts, it is then possible to extract the forward rate constant for the cyclization step, Table 2. Inspection of these results shows no significant change in either forward or reverse reaction rates over two units of pH. Thus, the pK_a of the full ester product, P_4, has not been incorporated into the model. This pK_a must be below 6 which is on the same order (pK_a = 4.6−7.5) determined for the esters of **1** with various sugars.[9] Finally, the ring-closing step at high pH, $P_3 \rightarrow P_4$, may be estimated to have a $K_3 \sim 2 \times 10^{-11}$ M, revealing an unfavorable step in this reaction path.

CONCLUSIONS

A detailed investigation of the reaction between **1** and **ARS** was bolstered by kinetic studies. Examination of the progress curves for the association reactions done in aqueous solution at pH from 4 to 10.5 revealed an initial process approaching equilibrium within 5−10 s. The minimum reaction mechanism for the first of two phases requires three parallel reaction paths connected by reactant and/or product ionizations (Figure 8). The first dehydration reaction yields a set of three related products (P_1−P_3) connected by two ionizations, pK_a's of 4.7 and 10.3. At each pH, the preferred reaction course depends on both reactant pK_a's (6.0 and 11.0 for **ARS**; 9.2 for **1**) as well as the relative kinetics of the paths. The preferred path, at near neutral pH, has an association constant of 2250 M^{-1} and a forward rate of 195 M^{-1} s^{-1} and is the reaction between the monodeprotonated **ARS** (A_1) and the neutral, trigonal **1** (B_1). The other reaction paths, at low and high pH, proceed with association constants and rates an order of magnitude less, 34 and 200 M^{-1} and 12 and 16 M^{-1} s^{-1}, respectively, with in both cases. These results reveal that, in the reaction with **ARS**, both trigonal and tetrahedral forms of **1** are reactive, however the trigonal form is more reactive by an order of magnitude.

Formation of the diester adduct that is tetrahedral about boron (P_4) resulting from the second phase, an intramolecular dehydration reaction, could not be observed directly. Therefore, this adduct was accessed synthetically and the dissociation reaction was monitored upon its mixing with aqueous buffer at pH's of 6−8. It was observed that the P_4 to P_2 reaction approaches equilibrium within 20 s and the P_2 to A_1 and B_1 equilibrium is reached much more slowly. These experiments yielded the kinetics of the reverse reaction (k_{-4} = 0.33 s^{-1} and k_{-1} = 0.09 s^{-1}) which, when combined with the previously determined forward kinetics and steady-state ^{11}B-NMR titration data, allowed for the calculation of the formation kinetics of this diester adduct, k_4 = 0.15 s^{-1}. These data indicate that this product (P_4) exists in facile equilibrium with the intermediate, monoester adduct (P_2) and in a ratio of approximately 2:1 (P_2:P_4). Additionally, the ionization of P_4 was not detected; therefore, it is concluded that this compound's pK_a is less than 6.

Additionally, this work made it possible to deduce the likely adduct structure responsible for the majority of the observed fluorescence. The steady-state experiments (fluorescence lifetimes and fluorescence and ^{11}B NMR titrations) indicated a minimum of two species being responsible for the observed fluorescence. The two species have been assigned as the monoester adduct (P_2) which is trigonal about boron and the diester, cyclic adduct (P_4) which is tetrahedral about boron (Figure 8). In aqueous solution near pH 7.5, these two species exist in an approximate molar ratio of 2:1 with a fluorescence ratio of 9:1, respectively. These structural assignments are consistent with what is known about the fluorescent contributions of boronic acids to conjugated systems. Most importantly, the diester, cyclic structure (P_4), the previously assumed sole fluorescent product,[9,37,47] was shown to be only a minor contributor to the reaction overall and the resulting fluorescence signal in particular.

In summary, the full mechanism of the reaction between phenylboronic acid (**1**) and Alizarin Red S (**ARS**) in aqueous solution at pH from 4 to 10.5 has been elucidated by the use of an array of steady-state and presteady-state methods. The reaction proceeds in two steps: the first step is complete within seconds and contributes the majority of observed fluorescence; while the second step is much slower (many tens of seconds) and is only a minor contributor to the fluorescence. The reaction path is also quite dependent upon the pH of the solution. The kinetically preferred reaction occurs at near-neutral pH and is the result of the neutral, trigonal species of **1** reacting with the monodeprotonated form of **ARS**. Thus, the trigonal form of 1 predominates in reactivity by an order of magnitude; however, the tetrahedral form contributes measurably. Finally, the full-ester adduct, previously the only assumed

adduct, has been shown to be only a minor contributor to the reaction overall.

EXPERIMENTAL SECTION

All reagents, including phenylboronic acid (**1**) and Alizarin Red S (**ARS**), were purchased commercially and were of the highest purity available. **ARS** and all buffer solutions were prepared with double-deionized water in triple-rinsed, acid-washed glassware. The **ARS** stock solution was 10 mM and was protected from light. All aqueous solutions were filtered through 0.45 μm Supor syringe filters. Stock solutions of **1** were 200 mM in DMSO. **1** was analyzed by ^{11}B NMR, found to be free of boric acid contamination, and was used as received. All solutions were stored at 4 °C in polypropylene tubes. Unless otherwise noted, all data were plotted and analyzed using KaleidaGraph v.3.5 by Synergy Software.

Buffers were prepared as 500 mM stock solutions and adjusted to final pH as indicated with either HCl or NaOH/glycine (pH = 3.0 and 3.5), acetic acid−sodium acetate (pH = 4.0, 4.5 and 5.0), MES (pH = 5.5, 6.0, and 6.5), HEPES (pH = 7.0, 7.5, and 8.0), CHES (pH = 8.6, 9.0, 9.5, and 10.0), and CAPS (pH = 10.5 and 11.0). Final solution pH was determined by preparing mock solutions (5 mL, lacking only compounds) and measuring pH with a pH meter calibrated against aqueous buffer solutions using a combination electrode without correction for liquid junction potentials.

UV/vis Spectra Collection. Solutions were placed into 1 mL quartz cuvettes, and spectral scans (1 nm resolution) were taken at room temperature. Scans were taken in the following regions: 240−340 nm for **1**; 240−700 nm for **ARS**; 350−700 nm for **1:ARS**. Solutions consisted of 1 mM **1**, 100 μM **ARS**, or 8 mM **1** and 100 μM **ARS**, respectively. All solutions contained 4% v/v DMSO and any one of 100 mM HCl, 100 mM NaOH, or 50 mM buffer. Ionization constants were derived from these data by the method of Tomsho et al.[53]

Fluorescence Spectra Collection. Measurements were collected at room temperature. Emission scans were taken from 460 to 800 nm with an excitation wavelength of 440 nm. Excitation scans were then taken from 300 to 550 nm with an emission wavelength equal to the wavelength of maximum fluorescence determined in the emission scan. All slit widths were set to 2 nm. Solutions consisted of 20 μM **ARS**, 4% v/v DMSO, 0 or 2 mM **1**, and any one of 100 mM HCl, 100 mM NaOH, or 50 mM buffer.

Fluorescence Lifetime (TCSPC) Determination. Data were collected at room temperature with a NanoLED-495 excitation source (1 MHz refresh rate) while the emission wavelength was set to 590 nm (20 nm bandpass). Data were collected with Data Station v. 2.5 and analysis was done with DAS6 software. Solutions consisted of 20 μM **ARS**, 2 mM **1**, 4% v/v DMSO, and 50 mM buffer (pH 4−10). Ludox CL colloidal silica solutions were used as light scattering standards.

Steady-State Fluorescence Titrations. Measurements were collected at 25.0 °C with excitation at 460 nm and emission at 590 nm utilizing 5 nm slit widths. The K_a of the **1:ARS** complex was determined by two-component fluorescent titrations by the method of Springsteen and Wang.[9] The K_a values were determined by fitting the data to eq 2. These samples contained 50 mM buffer, 5% v/v DMSO, 20 μM ARS, and 0−10 mM **1** in ddH_2O. An ARS solution and solutions of all other components except for ARS were prepared and equilibrated at 25.0 °C in separate vessels. Upon ARS solution addition, the complete reaction solution was mixed well and maintained in the dark at 25.0 °C for 3 min prior to the measurement of fluorescence.

^{11}B NMR. Spectra were collected at 96.21 MHz using a 4.9 μs 90° pulse, 488 ms FID acquisition time, and a 1 s acquisition delay. The sweep width was set to 87.2 ppm and the temperature to 25.0 °C. All chemical shifts were referenced to an external standard of $BF_3(Et_2O)$ at 0.0 ppm. Samples were prepared in 10% v/v D_2O in ddH_2O as the lock solvent and were placed into quartz NMR tubes. Each sample consisted of 50 mM buffer, 7.5−10 mM boron compound, and 0−7.5 mM ARS. Two thousand scans were taken for each sample and the data were then processed using SpinWorks v.2.5.5. A minimum of three independent determinations were made at each pH examined from 5 to 10.

Preparation of the 1:ARS Full-Ester Adduct (P4). Using standard procedures to exclude moisture, Alizarin Red S (173 mg, 0.5 mmol), phenylboronic acid (67 mg, 0.5 mmol), and anhydrous potassium carbonate (173 mg, 1.25 mmol) were sealed in a round bottomed flask under an argon atmosphere. To this was added 10 mL of acetonitrile (dried by stirring over anhydrous potassium carbonate under argon), and the resulting suspension was stirred vigorously for ~18 h at room temperature in the dark. Stirring was stopped, and the suspension was allowed to settle. Using dry needles, syringes, and syringe filters, the supernatant was removed and filtered through a 0.45 μm nylon syringe filter taking care to minimize solution exposure to air. The solution was protected from light and used immediately: ^{1}H NMR (CD_3CN) δ 8.28 (m, 2H), 8.04 (dd, 60H), 7.88 (dd, 31H), 7.75 (dd, 60H), 7.54 (dd, 31H), 7.39 (m, 245H), 7.13 (t, 31H), 7.03 (t, 16H), 6.06 (s, 58H); ^{11}B NMR (CD_3CN) δ 29.96 (4.51), 5.26 (1.00), 2.26 (0.014); λ_{max} (CH_3CN) 454 nm.

Presteady-State Kinetics. *(1) Forward Reaction Kinetic Determinations.* Reaction progress was monitored on a stopped-flow reaction analyzer with fluorescence detection. The excitation wavelength was 450 nm with a 4.65 nm slit width, emission was monitored with the use of an OG530 nm long wave pass filter, temperature was controlled at 25.0 ± 0.1 °C, and reaction progress was followed for up to 100 s. For each pH and boron compound concentration examined, two solution sets were prepared such that all contained 50 mM buffer and 4% v/v DMSO in ddH_2O. The ARS solution additionally contained 0.2 mM ARS while the boron compound solutions contained 0−8 mM compound; in both cases the final concentrations of both the ARS and boron compounds are halved upon mixing for reaction initiation. Reaction progress curves were analyzed using the Applied Photophysics Pro-Data Viewer v. 4.2.0 for fitting to a single exponential curve to obtain apparent rate data.

(2) pH-Jump and -Drop Experiments. The stopped-flow instrumental setup was as detailed for the forward reaction kinetic determinations above except UV/vis data was additionally collected using photodiode array detection. The **1:ARS** adduct was formed in situ at pH 6.0, 7.5, or 9.0 by preparing a solution containing 0.2 mM **ARS** and 8 mM **1** in 20 mM buffer. This solution was kept in the dark and allowed to age at room temperature for at least 15 min prior to first use. To achieve the desired pH change, this solution was diluted into 200 mM buffer of the desired pH, NaOH, or HCl. All solutions were 4% v/v DMSO in ddH_2O. As above, the final concentrations of all solutions are halved upon mixing for reaction initiation. Final solution pH, after mixing, was determined by preparation of a mock solution whose pH was measured. Reaction progress curves were analyzed using the Applied Photophysics Pro-Data Viewer v. 4.2.0 for fitting to a single exponential curve to obtain apparent rate data. Photodiode array data was analyzed using the Applied Photophysics Pro-Kineticist v. 1.0.8.

(3) Reverse Reaction Kinetic Determinations. The stopped-flow instrumental setup was as detailed for the forward reaction kinetic determinations above except the instrument was configured for asymmetric mixing with a ratio of 1:25 and data collection up to 60 s. The **1:ARS** full-ester adduct solution in acetonitrile is freshly prepared as described above. Buffer solutions, 50 mM in ddH_2O, of the desired pHs (6−8) are prepared. Mixing for reaction initiation results in a 25-fold dilution of the **1:ARS** full-ester adduct solution into buffer resulting in 4% v/v acetonitrile final. Reaction progress curves were analyzed using the Applied Photophysics Pro-Data Viewer v. 4.2.0 for fitting to a double exponential curve to obtain apparent rate data.

ASSOCIATED CONTENT

Supporting Information

Spectral data for the pK_a determinations of **1**, **ARS**, and the **1:ARS** complex; NMR spectra for the synthesis of the **1:ARS** diester adduct in acetonitrile; spectral comparisons for pH-jump and -drop experiments; ^{11}B NMR integration data and K_2

dx.doi.org/10.1021/jo202250d | J. Org. Chem. 2012, 77, 2098−2106

calculation; derivations for eqs 3−6. This material is available free of charge via the Internet at http://pubs.acs.org.

AUTHOR INFORMATION

Corresponding Author

*E-mail: sjb1@psu.edu.

ACKNOWLEDGMENTS

We thank Dr. Tony Liu for a critical review of the manuscript.

REFERENCES

(1) Lorand, J. P.; Edwards, J. O. *J. Org. Chem.* **1959**, *24*, 769−774.
(2) Hall, D. G. *Boronic Acids*; Wiley-VCH: Weinheim, 2005.
(3) James, T. D. *Top. Curr. Chem.* **2007**, *277*, 107−152.
(4) Jin, S.; Cheng, Y. F.; Reid, S.; Li, M. Y.; Wang, B. H. *Med. Res. Rev.* **2010**, *30*, 171−257.
(5) Galbraith, E.; James, T. D. *Chem. Soc. Rev.* **2010**, *39*, 3831−3842.
(6) Nishiyabu, R.; Kubo, Y.; James, T. D.; Fossey, J. S. *Chem. Commun.* **2011**, *47*, 1106−1123.
(7) Van Duin, M.; Peters, J. A.; Kieboom, A. P. G; Van Bekkum, H. *Tetrahedron* **1984**, *40*, 2901−2911.
(8) Van Duin, M.; Peters, J. A.; Kieboom, A. P. G; Van Bekkum, H. *Tetrahedron* **1985**, *41*, 3411−3421.
(9) Springsteen, G.; Wang, B. H. *Tetrahedron* **2002**, *58*, 5291−5300.
(10) Yan, J.; Springsteen, G.; Deeter, S.; Wang, B. H. *Tetrahedron* **2004**, *60*, 11205−11209.
(11) Babcock, L.; Pizer, R. *Inorg. Chem.* **1980**, *19*, 56−61.
(12) Pizer, R.; Tihal, C. *Inorg. Chem.* **1992**, *31*, 3243−3247.
(13) Pizer, R. D.; Tihal, C. A. *Polyhedron* **1996**, *15*, 3411−3416.
(14) Bishop, M.; Shahid, N.; Yang, J. Z.; Barron, A. R. *Dalton Trans.* **2004**, 2621−2634.
(15) Rietjens, M.; Steenbergen, P. A. *Eur. J. Inorg. Chem.* **2005**, 1162−1174.
(16) Iwatsuki, S.; Nakajima, S.; Inamo, M.; Takagi, H. D.; Ishihara, K. *Inorg. Chem.* **2007**, *46*, 354−356.
(17) Miyamoto, C.; Suzuki, K.; Iwatsuki, S.; Inamo, M.; Takagi, H. D.; Ishihara, K. *Inorg. Chem.* **2008**, *47*, 1417−1419.
(18) Groziak, M. P. *Am. J. Therapeutics* **2001**, *8*, 321−328.
(19) Yang, W.; Gao, X.; Wang, B. H. *Med. Res. Rev.* **2003**, *23*, 346−368.
(20) Ali, H. A.; Dembitsky, V.; Srebnik, M. *Contemporary Aspects of Boron: Chemistry and Biological Applications*; Elsevier: Amsterdam, 2005; Vol. *22*.
(21) Hunter, P. *EMBO Rep.* **2009**, *10*, 125−128.
(22) Baker, S. J.; Tomsho, J. W.; Benkovic, S. J. *Chem. Soc. Rev.* **2011**, *40*, 4279.
(23) Adams, J.; Kauffman, M. *Cancer Investigation* **2004**, *22*, 304−311.
(24) Crompton, I. E.; Cuthbert, B. K.; Lowe, G.; Waley, S. G. *Biochem. J.* **1988**, *251*, 453−459.
(25) Priestley, E. S.; De Lucca, I.; Ghavimi, B.; Erickson-Viitanen, S.; Decicco, C. P. *Bioorg. Med. Chem. Lett.* **2002**, *12*, 3199−3202.
(26) Fevig, J. M.; Buriak, J.; Cacciola, J.; Alexander, R. S.; Kettner, C. A.; Knabb, R. M.; Pruitt, J. R.; Weber, P. C.; Wexler, R. R. *Bioorg. Med. Chem. Lett.* **1998**, *8*, 301−306.
(27) Albers, H. M. H. G.; Hendrickx, L. J. D.; van Tol, R. J. P.; Hausmann, J.; Perrakis, A.; Ovaa, H. *J. Med. Chem.* **2011**, *54*, 4619−4626.
(28) Baggio, R.; Elbaum, D.; Kanyo, Z. F.; Carroll, P. J.; Cavalli, R. C.; Ash, D. E.; Christianson, D. W. *J. Am. Chem. Soc.* **1997**, *119*, 8107−8108.
(29) London, R. E.; Gabel, S. A. *Arch. Biochem. Biophys.* **2001**, *385*, 250−258.
(30) Asano, T.; Nakamura, H.; Uehara, Y.; Yamamoto, Y. *ChemBioChem* **2004**, *5*, 483−490.
(31) Minkkila, A.; Saario, S. M.; Kasnanen, H.; Leppanen, J.; Poso, A.; Nevalainen, T. *J. Med. Chem.* **2008**, *51*, 7057−7060.
(32) Rock, F. L.; Mao, W. M.; Yaremchuk, A.; Tukalo, M.; Crepin, T.; Zhou, H. C.; Zhang, Y. K.; Hernandez, V.; Akama, T.; Baker, S. J.; Plattner, J. J.; Shapiro, L.; Martinis, S. A.; Benkovic, S. J.; Cusack, S.; Alley, M. R. K. *Science* **2007**, *316*, 1759−1761.
(33) Zervosen, A.; Herman, R.; Kerff, F.; Herman, A.; Bouillez, A.; Prati, F.; Pratt, R. F.; Frere, J. M.; Joris, B.; Luxen, A.; Chaelier, P.; Sauvage, E. *J. Am. Chem. Soc.* **2011**, *133*, 10839−10848.
(34) Szebellady, L.; Tomay, S. *Z. Anal. Chem.* **1936**, *107*, 26.
(35) Campana, A. M. G.; Barrero, F. A.; Ceba, M. R. *Analyst* **1992**, *117*, 1189−1191.
(36) Chimpalee, N.; Chimpalee, D.; Boonyanitchayakul, B.; Burns, D. T. *Anal. Chim. Acta* **1993**, *282*, 643−646.
(37) Springsteen, G.; Wang, B. H. *Chem. Commun.* **2001**, 1608−1609.
(38) Kubo, Y.; Ishida, T.; Kobayashi, A.; James, T. D. *J. Mater. Chem.* **2005**, *15*, 2889−2895.
(39) Nonaka, A.; Horie, S.; James, T. D.; Kubo, Y. *Org. Biomol. Chem.* **2008**, *6*, 3621−3625.
(40) Bosch, L. I.; Fyles, T. M.; James, T. D. *Tetrahedron* **2004**, *60*, 11175−11190.
(41) Good, N. E.; Winget, G. D.; Winter, W.; Connolly, T. N.; Izawa, S.; Singh, R. M. M. *Biochemistry* **1966**, *5*, 467−&.
(42) Sabins, R. W. *Handbook of Acid−Base Indicators*; CRC Press: Boca Raton, 2008.
(43) Chapelle, S.; Verchere, J. F. *Tetrahedron* **1988**, *44*, 4469−4482.
(44) Baldwin, J. E.; Claridge, T. D. W.; Derome, A. E.; Schofield, C. J.; Smith, B. D. *Bioorg. Med. Chem. Lett.* **1991**, *1*, 9−12.
(45) Harris, W. R.; Amin, S. A.; Kupper, F. C.; Green, D. H.; Carrano, C. J. *J. Am. Chem. Soc.* **2007**, *129*, 12263−12271.
(46) Berube, M.; Dowlut, M.; Hall, D. G. *J. Org. Chem.* **2008**, *73*, 6471−6479.
(47) Kubo, Y.; Kobayashi, A.; Ishida, T.; Misawa, Y.; James, T. D. *Chem. Commun.* **2005**, 2846−2848.
(48) Doskocz, M.; Kubas, K.; Frackowiak, A.; Gancarz, R. *Polyhedron* **2009**, *28*, 2201−2205.
(49) Fain, V. Y.; Zaitsev, B. E.; Ryabov, M. A. *Russ. J. Gen. Chem.* **2004**, *74*, 1558−1563.
(50) Huebner, A.; Qu, Z. W.; Englert, U.; Bolte, M.; Lerner, H. W.; Holthausen, M. C.; Wagner, M. *J. Am. Chem. Soc.* **2011**, *133*, 4596−4609.
(51) DiCesare, N.; Lakowicz, J. R. *J. Phys. Chem. A* **2001**, *105*, 6834−6840.
(52) Yoon, J.; Czarnik, A. W. *J. Am. Chem. Soc.* **1992**, *114*, 5874−5875.
(53) Tomsho, J. W.; Pal, A.; Hall, D. G.; Benkovic, S. J. *ACS Med. Chem. Lett.* **2012**, *3*, 48.